Optical-Model Analysis of Elastic Scattering of Protons on Oxygen at Intermediate Energies*

C. B. DUKE
Palmer Physical Laboratory, Princeton University, Princeton, New Jersey
(Received 1 August 1962)

Differential cross sections and polarizations for the elastic scattering of protons by oxygen at bombarding energies between 8.66 and 19.2 MeV have been analyzed using the diffuse-surface optical model of the nucleus. The best fits to the experimental data were obtained by a least-squares procedure. Excellent fits to the experimental differential cross sections were obtained over almost the entire region, although resonance structures in the cross sections required a rapid variation of the parameters with energy. The presence of a thin absorptive shell and small volume absorption is the outstanding feature of the optical potential. A Thomas spin-orbit term did not satisfactorily reproduce the experimental polarizations.

I. INTRODUCTION

A PREVIOUS analysis[1] (to be referred to as NDM) of the angular distributions, polarizations, and reaction cross sections of medium energy protons elastically scattered by carbon indicated that the nuclear optical model was surprisingly successful in accounting for the experimental data. In order to ascertain whether the success of the model was fortuitous in the carbon analysis or possibly a general feature of elastic proton scattering from light nuclei, it was decided to undertake the analysis of data from another light nucleus. Oxygen was selected for several reasons. First, a large quantity of experimental differential cross sections taken at small energy intervals was available in the intermediate energy region. Second, these data revealed regions in which the structure of the differential cross sections changed rapidly over small energy intervals. These regions, which will be called resonance regions, have previously been treated both by the inclusion of an additional term in the scattering amplitude[2] and by consideration as giant resonances.[2,3] It was felt that a detailed analysis of these regions in terms of the nuclear optical model was desirable both in order to ascertain whether the model could account for the experimental data, and in order to investigate the behavior of the model parameters in the neighborhood of the resonances. Finally, as the absorptive part of the optical potential has been linked to the structure of the nuclear surface,[4] it was desired to obtain a precise evaluation of this absorptive potential over a moderate range of energy which included resonance regions.

A detailed analysis of the oxygen elastic scattering data over the energy range $8.66 \leq E_{\text{lab}} < 19.2$ MeV indicates that good fits to the experimental data can be obtained throughout this region except between 11 and 12 MeV. The resonances in the differential cross sections cause the parameters and partial-wave absorption cross sections to exhibit certain characteristic structures as functions of energy. In particular, the parameters vary more severely as functions of energy here than in the carbon analysis[1] so that the applicability of an optical-model analysis of the data is less certain.

II. EXPERIMENTAL DATA

One of the primary reasons for analyzing elastic proton scattering by oxygen was the availability of a considerable quantity of differential cross-section data at bombarding energies below 20 Mev.[3,5–10] Unfortunately, polarization data[11–13] are less plentiful in this region. The analysis was restricted to the energy region $8.66 \leq E_{\text{lab}} \leq 19.2$ MeV both for consistency with the

TABLE I. Experimental data on elastic p-O scattering used in the analysis.

Laboratory	Reference	E_{lab}(MeV)
Differential elastic scattering cross sections		
Tokyo	3	8.66, 9.42, 10.2, 10.5, 10.8, 11.1, 11.4, 11.9, 12.9, 13.9, 14.3, 14.5, 14.7, 15.2, 15.6
Tokyo	7	14.1
Princeton	9	15.2, 16.0, 16.4, 17.0, 17.4, 18.0, 18.4, 19.2
Polarizations		
Los Alamos	12	10

* This work was supported by the U. S. Atomic Energy Commission and the Higgins Scientific Trust Fund.

[1] J. S. Nodvik, C. B. Duke, and M. A. Melkanoff, Phys. Rev. 125, 975 (1962).

[2] B. R. Easlea, University of London, Ph.D. thesis, 1961 (unpublished).

[3] S. Kobayashi, J. Phys. Soc. Japan 15, 1164 (1960).

[4] See, for example, P. E. Hodson, in *Proceedings of the Rutherford Jubilee International Conference, Manchester, 1961*, edited by J. B. Berks (Academic Press Inc., New York, 1961), p. 357.

[5] W. E. Burcham, W. M. Gibson, A. Hossain, and J. Roblat, Phys. Rev. 92, 1266 (1953).

[6] W. M. Gibson, D. J. Prowse, and J. Roblat, Proc. Roy. Soc. (London) Ser. A 234, 237 (1957).

[7] C. Hu, K. Kikuchi, S. Kobayashi, K. Matsuda, Y. Nagahara, Y. Oda, N. Takano, M. Takeda, and T. Yamazaki, J. Phys. Soc. Japan 14, 861 (1959); S. Kobayashi (private communication).

[8] D. R. Maxson, Phys. Rev. 123, 1304 (1961).

[9] W. Daehnick and J. Christenson (preliminary data).

[10] G. Hardie (private communication); S. R. Salisbury, G. Hardie, L. Oppliger, and R. Dangle (to be published); G. Hardie and H. T. Richards, Bull. Am. Phys. Soc. 7, 289 (1962).

[11] L. Rosen, J. E. Brolley, Jr., M. L. Gursky, and L. Stewart, Phys. Rev. 124, 199 (1961).

[12] L. Rosen, J. E. Brolley, Jr., and L. Stewart, Phys. Rev. 121, 1423 (1961).

[13] L. Stewart (private communication).

TABLE II. Optical-model parameters corresponding to optimum fits.

E_{lab} (MeV)	R_0 (F)	b (F)	W (MeV)	W_1 (MeV)	V (MeV)	V_S (MeV)	a (F)	σ_r (mb)	χ_0^2
8.66	1.25	0.8	0	1.4	52.7	7.8	0.38	185	36
9.42	1.25	0.8	0	0.8	52.3	7.7	0.31	121	263
10.2	1.25	0.4	0	4.3	51.7	6.9	0.38	243	226
10.5	1.25	0.6	0	1.9	52.4	8.0	0.38	276	65
10.8	1.25	1.0	0	3.0	48.8	4.7	0.59	385	198
11.1[a]	1.30	0.8	0	5.2	43.5	2.7	0.69	529	491
11.4[a]	1.30	0.4	0	6.7	44.7	4.6	0.57	375	352
11.9	1.25	0.4	0	8.6	49.2	5.4	0.61	436	364
12.9	1.25	0.2	0	17.3	49.1	4.8	0.57	405	93
13.9	1.25	0.2	0	16.6	50.0	4.9	0.55	396	129
14.1	1.25	0.2	0	16.8	50.2	5.2	0.52	389	171
14.3	1.20	1.0	0	4.0	51.9	4.9	0.55	429	52
14.5	1.20	1.0	0	3.2	52.2	4.2	0.53	373	38
14.7[a]	1.20	0.6	4	0.4	53.1	4.2	0.58	409	11
15.2	1.25	2.4	0	1.8	47.8	4.6	0.57	551	81
15.6	1.25	1.6	0	2.9	49.2	6.6	0.62	516	24
16.0	1.25	0.2	0	14.2	52.3	12.1	0.46	254	1017
16.4	1.25	0.2	0	22.6	45.7	11.7	0.61	406	523
17.0	1.25	0.2	0	28.0	47.5	12.3	0.60	435	260
17.4[a]	1.25	0.8	0	5.7	47.6	4.0	0.52	434	78
18.0	1.25	1.4	0	3.6	44.7	2.3	0.55	491	815
18.4	1.25	1.2	0	4.8	46.4	2.4	0.57	516	498
19.2[a]	1.30	0.5	0	13.1	46.1	3.1	0.56	502	166

[a] A grid including $R_0=1.3$ F was employed in analyzing the data at this energy.

carbon analysis[1] and because the low-energy data are being treated elsewhere.[10] The experimental data which were used in the analysis are presented in Table I.

The method for determining the best fit to a set of data is based on a χ^2 test, described in NDM, which requires the assignment of an experimental error at every point. These errors were taken to be the quoted ones for the Tokyo data.[3,7] Smaller errors than the given experimental ones were assigned to the Princeton data[9] in the region of the first diffraction minimum in order to achieve consistent fits from one energy to another.

The major part of the analysis employed no polarization data at all. The 10-MeV polarization data were utilized together with the 10.2-MeV cross-section data only in one special calculation, which is discussed in Sec. VI D.

Experimental differential cross sections from both Princeton and Tokyo were available at 15.2 MeV and served as a convenient check on the energy normalizations of the two laboratories. Separate analyses of the two sets of 15.2-MeV data yielded almost identical optimum fit parameters, and only the results for the Tokyo data are given below.

III. INVESTIGATION OF THE OPTICAL-MODEL POTENTIALS

All of the optical-model potentials investigated are of the form

$$V_{OPT}=V_{CN}+V_{SO}+V_{Coul}, \tag{1}$$

where V_{CN} and V_{SO} are, respectively, the (complex) central nuclear and spin-orbit potentials, and the Coulomb potential, V_{Coul}, is that corresponding to a uniformly charged sphere of radius R. The real part of V_{CN} is given by

$$\mathrm{Re}(V_{CN})=-Vf(r), \tag{2}$$

where

$$f(r)=1+\exp[(r-R)/a]^{-1}, \tag{3}$$

and $R=R_0A^{1/3}$.

The imaginary part of the central potential was selected to be of the surface-plus-volume form[1]

$$\mathrm{Im}(V_{CN})=-W_1\exp[-(r-R)^2/b^2] -W\{1+\exp[(r-R)/0.69b]\}^{-1}, \tag{4}$$

the factor of 0.69 arising from the requirement that the volume term fall from 90 to 10% over that interval in which the Gaussian surface term exceeds 10% of its maximum value. This characterization of the absorptive potential avoids the introduction of an additional parameter.

The spin-orbit potential is given by

$$V_{SO}=-\left(\frac{\hbar}{m_\pi c}\right)^2(V_S+iW_S)\frac{1}{r}\frac{df}{dr}\boldsymbol{\sigma}\cdot\mathbf{l}. \tag{5}$$

In general, W_S was set equal to zero,[14] so that the potential is determined by the seven parameters V, W, W_1, V_S, R_0, a, and b. For most energies, however, only six parameters were required as the best fits resulted from the use of either pure surface or pure volume absorption.

IV. METHOD OF ANALYSIS

The cross sections and polarizations were calculated on the IBM 7090 computer at New York University

[14] Except in a special calculation at 10.2 MeV where polarization data were available.

TABLE III. Optical-model parameters corresponding to compromise fits.

E_{lab} (MeV)	R_0 (F)	b (F)	W (MeV)	W_1 (MeV)	V (MeV)	V_S (MeV)	a (F)	σ_r (mb)	χ_σ^2
8.66	1.25	0.6	0	1.8	52.6	7.7	0.38	174	40
9.42	1.25	0.6	0	1.1	52.3	7.7	0.32	119	270
10.2	1.25	0.6	0	3.0	51.6	6.9	0.38	253	234
10.5[a,b]	1.25	0.6	0	1.9	52.4	8.0	0.38	276	65
10.8	1.25	0.6	0	4.7	49.4	4.5	0.58	349	258
11.1	1.25	0.4	0	9.6	46.6	1.8	0.68	427	860
11.4	1.25	0.3	0	8.9	47.5	4.8	0.59	338	469
11.9	1.25	0.3	0	10.7	49.4	5.5	0.59	411	370
12.9	1.25	0.3	0	11.9	49.0	4.7	0.57	416	95
13.9	1.25	0.3	0	11.2	49.8	4.9	0.55	402	139
14.1	1.25	0.3	0	11.4	50.0	5.2	0.52	397	176
14.3[b]	1.25	0.6	0	5.8	49.7	4.6	0.51	403	69
14.5	1.25	0.6	2	2.6	49.4	3.8	0.50	400	81
14.7[b]	1.25	0.2	4	0.5	50.4	3.7	0.53	414	33
15.2	1.25	1.4	4	0.4	47.7	4.8	0.62	554	90
15.6	1.25	1.4	2	2.0	49.0	7.0	0.64	538	47
16.0	1.25	1.2	0	4.5	49.0	6.8	0.61	519	1077
16.4[a,b]	1.25	0.2	0	22.5	45.7	11.7	0.61	406	523
17.0[a,b]	1.25	0.2	0	28.0	47.5	12.3	0.60	435	260
17.4[a,b]	1.25	0.8	0	5.7	47.6	4.0	0.52	434	78
18.0	1.25	1.2	0	4.1	45.2	2.4	0.54	475	818
18.4[a,b]	1.25	1.2	0	4.8	46.4	2.3	0.57	516	498
19.2[b]	1.25	0.8	0	9.1	48.2	3.9	0.62	537	277

[a] Optimum and compromise fits coincide.
[b] The compromise fit is the optimum fit at $R_0=1.25$ F.

using the UCLA automatic search program.[1,15] The optimum fit to the experimental data is defined to be the one which minimizes the quantity χ^2 given by

$$\chi^2=\chi_\sigma^2+\chi_P^2, \tag{6}$$

where

$$\chi_\sigma^2=\sum_i\left[\frac{\sigma^{th}(\theta_i)-\sigma^{ex}(\theta_i)}{\Delta\sigma^{ex}(\theta_i)}\right]^2, \tag{7}$$

and

$$\chi_P^2=\sum_j\left[\frac{P^{th}(\theta_j)-P^{ex}(\theta_j)}{\Delta P^{ex}(\theta_j)}\right]^2. \tag{8}$$

The search program minimizes χ^2 by simultaneous variation of certain model parameters while the remaining parameters, called grid parameters, are held constant. The minimization procedure is discussed in detail in NDM. Both in NDM and in the present analysis, b, W, and R_0 were selected to be the grid parameters. The analysis at each energy was executed by constructing a three-dimensional grid of values for b, W, and R_0 and, at each point in the grid, minimizing χ^2 by allowing the remaining parameters to assume their "optimum" values.

An initial investigation of the 14–15 MeV region was made with the grid $R_0=1.20$, 1.25, 1.30 F; $W=0$, 2, 4 MeV; and $b=0.2$, 0.4, 0.6, 0.8, 1.0 F. The analysis disclosed that $R_0=1.30$ F gave unacceptable fits in this region so that subsequent grids were confined to $R_0=1.20$ and 1.25 F. Selected energies were analyzed using the initial grid, however, in order to investigate the validity of using the restricted one. The basic grids at a given value of R_0 were always extended until the optimum fit lay within the range of the grid. For example, in the 15-MeV region the grids had to be extended to $b=2.4$ F in order to encompass the optimum fit. Finally, more extensive grids were often used to investigate the region near the minimum of the χ^2 surface in more detail.

The optimum fits presented in Table II and Fig. 1 were obtained by selecting, from the total grid, that grid point at which the lowest value of χ^2 was obtained. Also, in order to study the energy dependence of the parameters, it was decided to sacrifice some of the quality of the fits and select compromise fits which minimized variations in R_0 and b from one energy to the next. The absence of polarization and reaction cross section data renders inapplicable the NDM method of choosing the compromise fits, and permits the use of the above somewhat arbitrary selection procedure. This procedure eliminates, to a great extent, the effects of coupling between R_0, b, and the other model parameters, and hence simplifies the interpretation of the energy dependence of the parameters. The resulting compromise fits are presented in Table III and Fig. 2. Each of these fits is associated with a particular grid point and hence occurs with the optimum values of V, V_S, W_1, and a for that grid point.

The significance of the numerical value of χ^2 in terms of visual fits to the data may be estimated by comparing the optimum and compromise fits. The correlation between the value of χ^2 and the visual quality of the fits depends upon the size of the experimental errors and the number of data points at a given energy. It is discussed in detail in NDM.

[15] M. A. Melkanoff, J. S. Nodvik, D. S. Saxon, and D. G. Cantor, *A Fortran Program for Elastic Scattering Analyses with the Nuclear Optical Model* (University of California Press, Berkeley and Los Angeles, California, 1961).

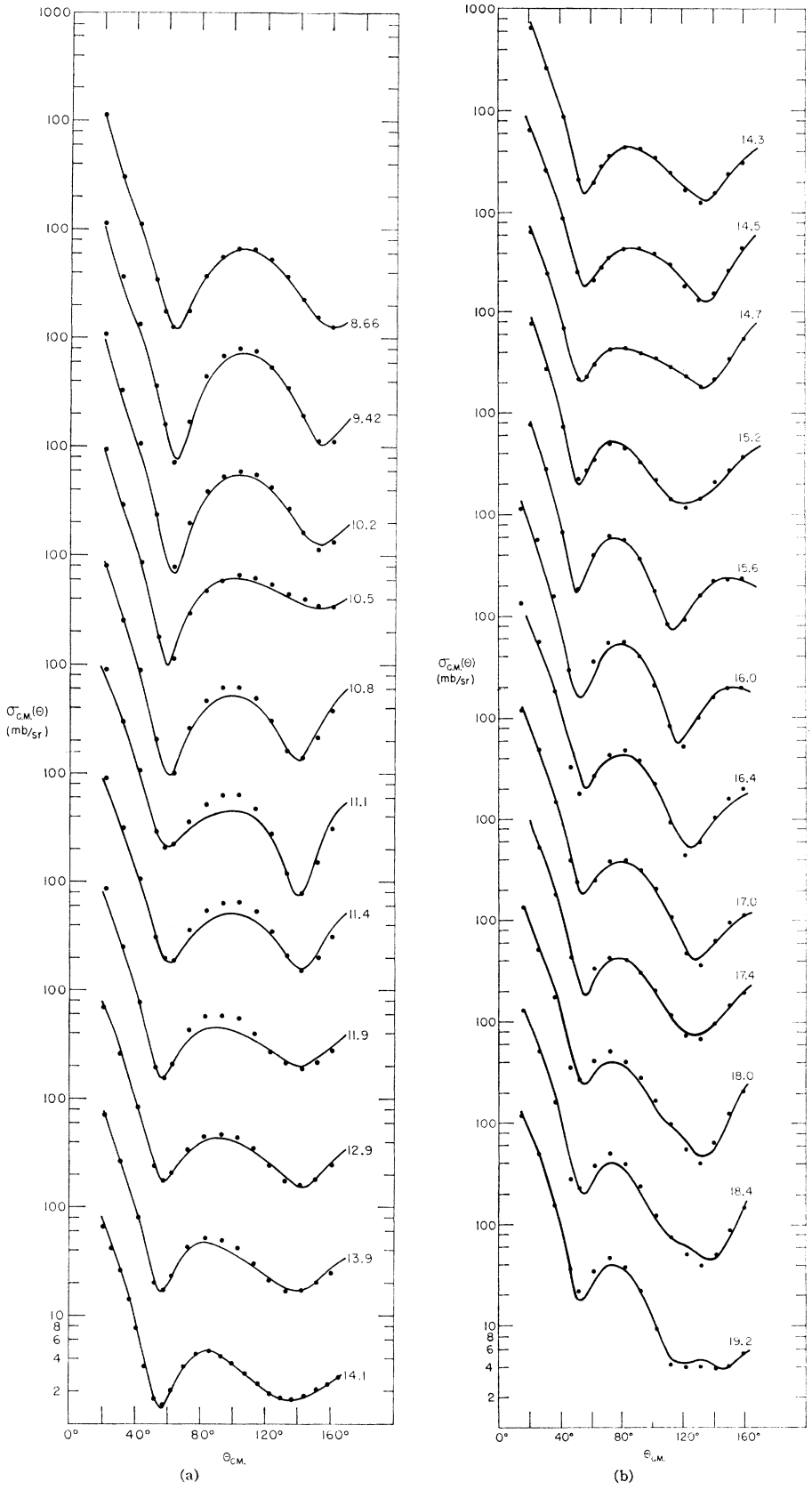

FIG. 1. Comparison of theoretical and experimental differential elastic scattering cross sections at various energies. The dots are experimental points. The solid lines are the optimum theoretical fits associated with the parameters given in Table II.

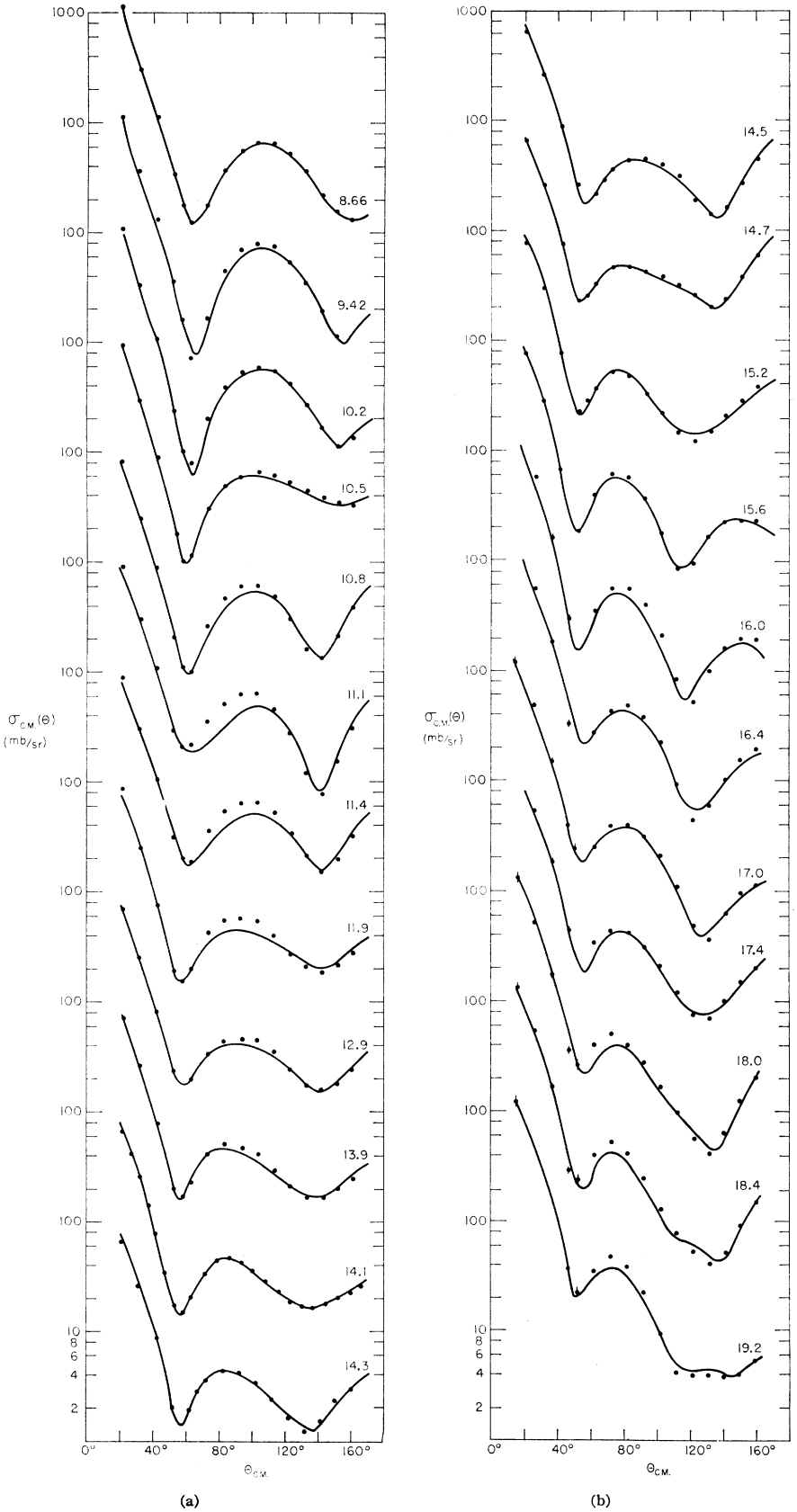

FIG. 2. Comparison of theoretical and experimental differential elastic scattering cross sections at various energies. The dots are experimental points. The solid lines are the compromise theoretical fits associated with the parameters given in Table III.

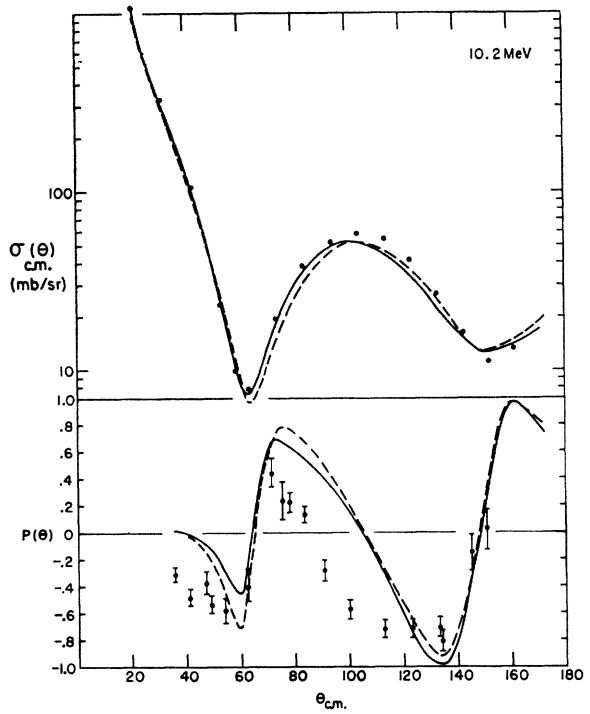

FIG. 3. Comparison of theoretical and experimental polarizations and differential elastic scattering cross sections at 10.2 MeV with the polarization data included in the χ^2 test. The solid lines represent the theoretical optimum fits when W_S is not constrained to zero, and are obtained from the parameters: $R_0=1.25$ F, $b=0.6$ F, $W=0$, $V=51$ MeV, $W_1=3.6$ MeV, $V_S=6.7$ MeV, $W_S=1.1$ MeV, $a=0.40$ F, $\chi_\sigma^2=217$, $\chi_P^2=608$. The dashed lines represent the theoretical optimum fits when W_S is set identically zero, and are obtained from the parameters: $R_0=1.25$ F, $b=0.6$ F, $W=0$, $V=51$ MeV, $W_1=3.4$ MeV, $V_S=6.7$ MeV, $a=0.40$ F, $\chi_\sigma^2=314$, $\chi_P^2=677$.

V. RESULTS

For the description and discussion of the results, it is convenient to arbitrarily divide the data into a low-energy region, $8.66\leq E_{\text{lab}}\leq 11.9$ MeV, and a medium energy region $11.9<E_{\text{lab}}\leq 19.2$ MeV.[16] The behavior of the cross sections as functions of energy in the low-energy region is seen most clearly from the Wisconsin data.[10] In particular, resonance behavior is observed at $E_{\text{lab}}=8.75$, 8.9, 9.9, and 10.5 MeV. The medium energy data are characterized by resonance structures at 12.4, 14.9, and 17.0 MeV.[9,17] Otherwise, the differential cross sections at a fixed angle seem to vary slowly with energy.

A. Low-Energy Analysis

Satisfactory fits to the experimental data were obtained for all energies in this region except 11.1 and 11.4 MeV. The outstanding characteristic of the model parameters is the absence of volume absorption even at the 10.5-MeV resonance. In fact, the demand for surface absorption is so pronounced at 10.5 MeV that the introduction of a 2-MeV volume absorption term increased χ^2 by a factor of 2 and caused W_1 to assume negative values. Such behavior is also a general feature of the results for energies below 10 MeV.

The radius parameter $R_0=1.25$ F proved to be quite satisfactory in the low-energy region. In the initial grid, all of the optimum fits occurred at this value of R_0, although subjectively better "visual" fits[18] could be obtained with $R_0=1.20$ in the 10-MeV region. Poor fits at 11.1 and 11.4 MeV required the extension of the grid to $R_0=1.30$ F at these energies, but the agreement with the experimental data remained poor.

The primary difficulty in the low-energy region occurred in trying to fit the data in the 11–12 MeV range. Measurements recently taken at Wisconsin[10] clearly indicate that the cross sections vary slowly with energy in this region. Hence, *a priori*, an optical-model analysis of the data appeared promising. However, an extensive grid encompassing $R_0=1.20$, 1.25, 1.30 F; $b=0.2$, 0.4, 0.6, 0.8, 1.0, 1.2 F, and $W=0$, 2, 4 MeV, with the regions of minimum χ^2 mapped out in more detail, failed to reveal any combination of parameters which could satisfactorily reproduce both the diffraction peak at $\theta_{\text{c.m.}}=100°$ and the deep minimum at $\theta_{\text{c.m.}}=140°$. Although these poor results may be partially due to scatter in the data,[19] the optical model reproduces the experimental data only qualitatively in the 11–12 MeV range. The combination of good fits at the 10.5-MeV resonance structure and significantly poorer ones in a region in which the cross sections vary slowly with energy is rather surprising, and is not yet understood.[20]

The results of fitting the 10.2-MeV cross-section data together with the 10-MeV polarizations are shown in Fig. 3, and will be discussed in Sec. VI D.

B. Medium-Energy Analysis

The region $11.9\leq E_{\text{lab}}\leq 14.1$ MeV proved to be quite similar to the comparable region in the carbon analysis[1] and is well described by a radius parameter $R_0=1.25$ F and a narrow surface absorption. Above 14.1 MeV, however, the differential cross sections begin to exhibit strong variations with energy,[9,17] and the results of the analysis become considerably more difficult to interpret.

A wide resonance structure, most clearly characterized by a maximum in the 160° cross sections, extends from 14.3 to about 16.0 MeV, with its peak located near 14.9 MeV.[3,17] The optical model was able to reproduce the angular distributions associated with this structure quite well provided that volume absorption

[16] The similarity of the dividing energy of ~12 MeV with that used in the carbon analysis is an interesting coincidence.

[17] W. Daehnick and J. Christenson, unpublished excitation functions of $O^{16}(p,p)O^{16}$ for $12\leq E_{\text{lab}}\leq 18$ MeV.

[18] Fits which reproduce the large-angle data more accurately at the expense of larger deviations from the data along the initial downward slope of the differential cross section.

[19] As indicated by a comparison of the data in references 3 and 10.

[20] This situation is reminiscent of that which B. R. Easlea found in Mg^{24} near 9.55 MeV. See reference 2.

was introduced into the potential. A strong preference for the lower value of $R_0=1.20$ F was indicated below 15 MeV, while above 15 MeV a larger radius parameter and an extremely wide surface was required. Both here and at the 10.5-MeV resonance a rapid rise in the computed reaction cross sections occurs at energies just above that at which the peak in the 160° differential cross sections is seen (see Tables II and III). In contrast to the 10.5-MeV structure, however, the presence of volume absorption is essential to the description of the data in the 14.7-MeV region. Therefore the two resonance regions, both superficially characterized by maxima in the large-angle differential cross sections, are described by the optical model in terms of quite different absorptive potentials.

The minimum in the large-angle cross sections[9,17] near 17.0 MeV is characterized by a deep, narrow surface absorption and a large spin-orbit potential. Furthermore, the 17.4–18 MeV region exhibits the increase in the reaction cross section which customarily follows a resonance structure. The surface absorption broadens out and the spin-orbit potential assumes lower values. The optimum and compromise fits are either identical or equivalent[21] within the energy range $16.4\leq E_{\text{lab}}\leq 18.4$ MeV.

In contrast to the carbon analysis[1] a single compromise value of b which gives satisfactory fits throughout the medium-energy region could not be found. The resonance structures in this region cause severe fluctuations in the values of b, W_1, W, and V_S which could be avoided only at the expense of obtaining unacceptable fits at several energies. A comparison between the theoretical and experimental differential cross sections is shown in Figs. 1 and 2.

VI. DISCUSSION

A. Uncertainty in the Parameters

In this analysis, only the uncertainties in the grid parameters R_0, b, and W were quantitatively investigated. If a single value of R_0 is required to fit the data over the entire energy range $8.66\leq E_{\text{lab}}\leq 19.2$ MeV, then this value is given by $R_0=1.25\pm 0.05$ F. The values of the other two grid parameters are harder to establish because of ambiguities which occur when several sets of parameters give equivalent fits to the experimental data.

The distribution of the absorptive potential between the surface and volume terms was investigated by plotting surfaces of constant χ^2 and constant reaction cross section as functions of the grid parameters b and W in Figs. 4–9. These figures were obtained for the radius parameter $R_0=1.25$ F. At any point on the figures, all of the other parameters, except R_0, assume values which minimize χ^2 for the fixed values of b and W associated with the selected point. The contours of constant reaction cross section display the accuracy needed in measurements of the reaction cross section before it can be used to determine the model parameters. The location and extent of the regions of minimal χ^2 permit an estimation of both of the relative amounts of surface and volume absorption in the neighborhood of the optimum fit, and of the ranges of b and W within which acceptable fits to the data can be found. In the low-energy region, the volume absorption term is less than 1 MeV deep, and the surface absorption has a width given by its optimum value (see Table II) with an acceptable spread of approximately $\Delta b=\pm 0.4$ F. The situation in the $11.9\leq E_{\text{lab}}\leq 14.1$ MeV region is shown in Fig. 4. The surfaces of constant χ^2 and constant reaction cross section at 12.9 MeV which are shown in this figure are typical of the entire region. However, the nature of the χ^2 and reaction cross-section contours changes drastically with energy near the 14.9-MeV resonance, so that this region is studied in detail in Figs. 5–9. The requirement of volume absorption quite close to the resonance is evident, as is the widening of the surface further away from the resonance with a concommitant ambiguity between a wide surface with no volume absorption and a somewhat narrower surface with 1 or 2 MeV of volume absorption. The χ^2 surfaces in the 17-MeV region resemble those of Fig. 4, while in the 18-MeV region they resemble Fig. 9. These figures give a quantitative meaning to the statement made in the last section that a single compromise value of b could not be found in the medium-energy region.

The grid-point method of analysis permits a detailed study to be made of the coupling between the grid parameters and the remaining search parameters, but does not yield much additional information on the search parameters themselves. For example, the analysis reveals a pronounced b-V coupling with the optimized value of V decreasing by 1–2 MeV with each 0.2 F increase in b in the 14.9-MeV region. The rate of decrease of V with respect to increases in b becomes smaller at lower energies, until at $10.2\text{ MeV}\leq E_{\text{lab}}\leq 8.66$ MeV, V begins to increase with increasing b. This type of energy-dependent coupling, which occurs between each grid parameter and most of the other parameters, illustrates the difficulties encountered in attempting to evaluate the uncertainties in the search parameters. A set of estimates of the range of variations of the individual search parameters which would produce equivalent fits to the data was given in NDM[22] and should be valid here also.

The influence of W_S on the quality of the fits was investigated by analyzing the 10.2-MeV cross-section data and the 10-MeV polarization data together; once setting $W_S=0$ and once allowing it to vary as a search parameter. The results are shown in Fig. 3. As the

[21] Fits to a given set of data which possess values of χ^2 within ± 10 of each other are considered equivalent.

[22] NDM, or M. A. Melkanoff, D. S. Saxon, and J. S. Nodvik, in *Proceedings of the Rutherford Jubilee International Conference, Manchester, 1961* (Academic Press Inc., New York, 1961), p. 411.

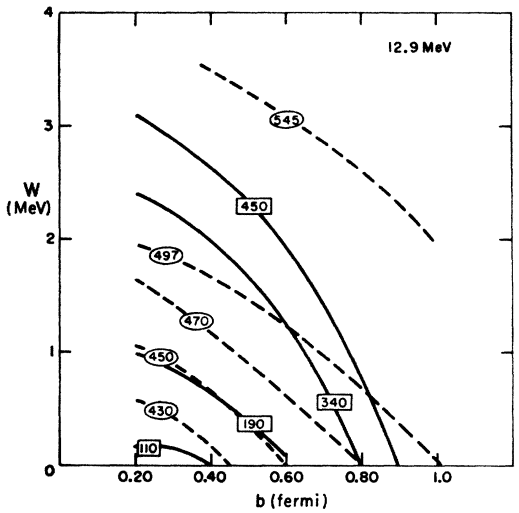

FIG. 4. Contours of constant χ^2 and reaction cross section in the b-W plane for $R_0=1.25$ F at 12.9 MeV. The solid curves are contours of constant χ^2 in the neighborhood of the optimum fit. The values of the other parameters are chosen to minimize χ^2 for given b, W, and R_0. The dashed curves are contours of constant σ_r(mb) obtained under the same conditions.

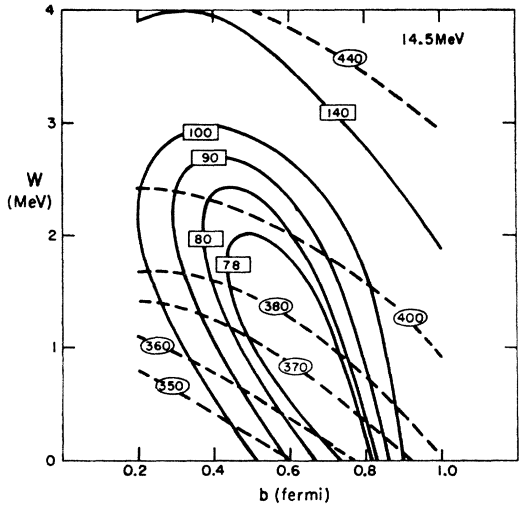

FIG. 6. Contours of constant χ^2 and reaction cross section in the b-W plane for $R_0=1.25$ F at 14.5 MeV. The solid curves are contours of constant χ^2, and the dashed curves are contours of constant σ_r(mb). The values of the other parameters are chosen to minimize χ^2 for given b, W, and R_0.

optimum value of $W_S\cong 1$ MeV reduces the value of χ^2 by only 11%, W_S appears to be relatively unimportant at this energy.

B. Energy Dependence of the Parameters

One of the outstanding features of the results of the analysis is the pre-eminence of a narrow surface absorption for most energies, with transitions to volume absorption or a much wider surface occurring only in certain regions in which the cross sections displayed extensive structure. This behavior of the absorptive potential is illustrated in Fig. 10. The predominance of surface absorption is emerging as a general feature of low- and medium-energy nucleon-nucleus elastic scattering.[1,23,24] An increase in absorption in the region of the nuclear surface is predicted even by such a simple model as the Fermi-gas model using the Thomas-Fermi local plane wave approximation to treat the surface region.[25] However, this calculation as well as the more sophisticated ones[26] overestimates the absorptive potential in the interior of the nucleus. This problem is currently being investigated as a first step in understanding the predominance of surface absorption.[27]

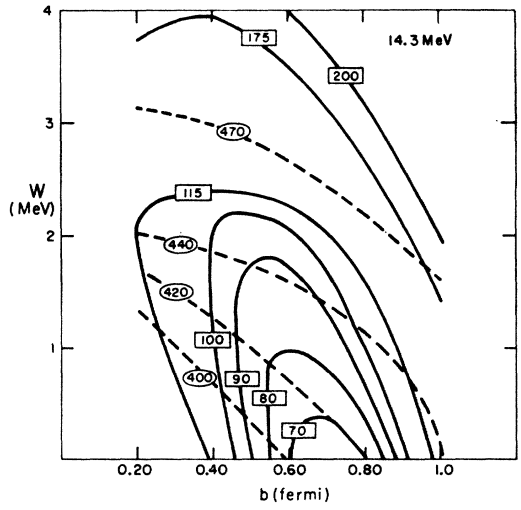

FIG. 5. Contours of constant χ^2 and reaction cross section in the b-W plane for $R_0=1.25$ F at 14.3 MeV. The solid curves are contours of constant χ^2, and the dashed curves are contours of constant σ_r(mb). The values of the other parameters are chosen to minimize χ^2 for given b, W, R_0.

The onset of pronounced structure in the differential cross sections above 14.1 MeV causes rapid changes in the nature of the absorptive potential. Tables II and III indicate wide fluctuations in the values of b, W, and W_1 in this region. Part of these fluctuations may be due to the onset of the (p,d) reaction at $E_{\text{lab}}=14.2$ MeV and the (p,n) reaction at 17.3 MeV. The thresholds for these reactions are correlated in an interesting fashion with variations in a as may be seen in Fig. 11. From this figure we also see that the product bW_1, which will be related to the reaction cross sections in the next section, is a relatively smooth function of energy as compared to either b or W_1 separately. However, for energies above 16.0 MeV, the values of b corresponding to the optimum fits depend sensitively upon the behavior of the differential cross sections for

[23] F. Bjorklund and S. Fernbach, in *Proceedings of the Second United Nations International Conference on the Peaceful Uses of Atomic Energy, Geneva, 1958* (United Nations, Geneva, 1958), Vol. XIV, p. 24.
[24] F. G. J. Perey and B. Buck, Nucl. Phys. **32**, 353 (1962).
[25] C. B. Duke (unpublished calculations).
[26] L. Verlet and J. Gavoret, Nuovo Cimento **10**, 505 (1958) and included references.
[27] E. P. Wigner and C. B. Duke (to be published).

$40° \leq \theta_{c\,m} \leq 60°$. Unfortunately, the differential cross section data are rather inaccurate at these angles, and a more precise experimental determination of these differential cross sections is needed before the χ^2 optimization procedure can give reliable optimum values of b within the energy range $16.0 \leq E_{lab} \leq 19.0$ MeV.

All of the differential cross-section data in the resonance regions can be described quite accurately by the optical model analysis, but only at the expense of considerable variations in the model parameters. The 14.9-MeV resonance structure resembles the one which occurred at 17.8 MeV in carbon.[1] The nature of the absorptive potential is drastically changed from surface to volume absorption with a concommitant sharp increase in the absorption of the lower partial waves due to the "filling in" of the nuclear interior. The 10.5- and 17.0-MeV structures are characterized by milder changes in the parameters whereby V_S increases; the absorptive potential remains sharp surface absorption; and a single partial wave ($f_{7/2}$ at 10.5 MeV and $d_{3/2}$ at 17.0 MeV) is suddenly strongly absorbed. The $f_{7/2}$ partial wave is also strongly absorbed at all energies above 12.0 MeV. In the optical-model analysis this absorption results from the radial structure of the absorptive potential and is not directly associated with the occurrence of resonances in the differential cross section in the $11 \leq E_{lab} \leq 15.6$ MeV region.[28]

An exceptionally good fit to the 10.5-MeV data, at the expense of only a slight variation in the parameters from the 10.2-MeV results, provoked a closer analysis of this region. A set of compromise parameters were

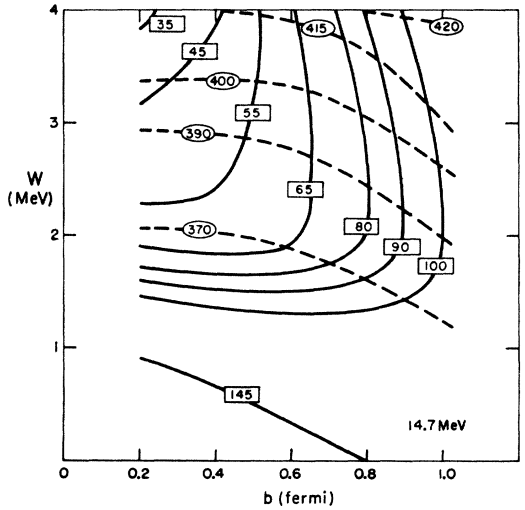

FIG. 7. Contours of constant χ^2 and reaction cross section in the b-W plane for $R_0 = 1.25$ F at 14.7 MeV. The solid curves are contours of constant χ^2, and the dashed curves are contours of constant σ_r(mb). The values of the other parameters are chosen to minimize χ^2 for given b, W, and R_0.

[28] Contrast this conclusion to those drawn in references 2 and 3 where a strong $l=3$ wave absorption is linked to a giant resonance in the 11–16 MeV region.

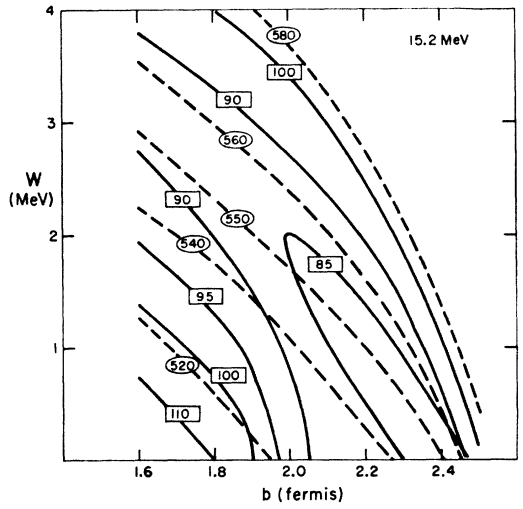

FIG. 8. Contours of constant χ^2 and reaction cross section in the b-W plane for $R_0 = 1.25$ F at 15.2 MeV. The solid curves are contours of constant χ^2, and the dashed curves are contours of constant σ_r(mb). The values of the other parameters are chosen to minimize χ^2 for given b, W, and R_0.

selected from the 10.2-, 10.5-, and 10.8-MeV optimum fits. The excitation functions predicted by these compromise parameters are compared in Fig. 12 to experimental excitation function[3,10] and to those predicted by the optimum-fit parameters. The figure clearly reveals that the 10.5-MeV results were obtained only at the expense of varying the parameters and that the resonance structure at this energy is not an inherent feature of the model, although the model is capable of reproducing it quite accurately by moderate variations of the parameters.

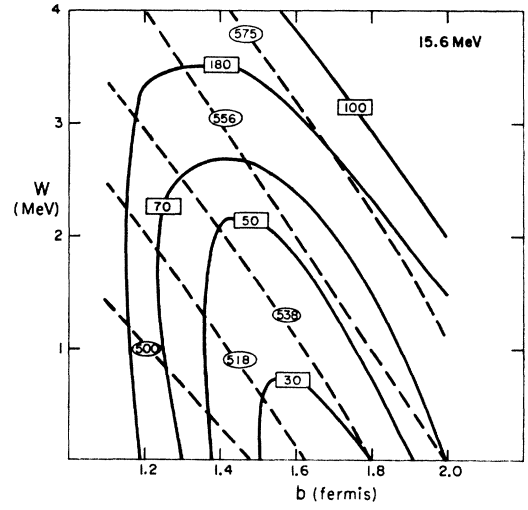

FIG. 9. Contours of constant χ^2 and reaction cross section in the b-W plane for $R_0 = 1.25$ F at 15.6 MeV. The solid curves are contours of constant χ^2, and the dashed curves are contours of constant σ_r(mb). The values of other parameters are chosen to minimize χ^2 for given b, W, and R_0.

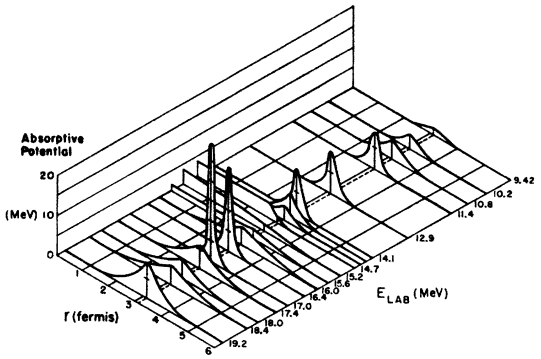

FIG. 10. Absorptive part of the optical-model potential corresponding to the compromise fits as a function of r and E_{lab} for $R_0=1.25$ F. The associated parameters are given in Table III.

C. Reaction Cross Sections

The values of the total reaction cross sections corresponding to the optimum and compromise fits are contained in Tables II and III, respectively. A search of the literature disclosed no measurements of these quantities in the region of interest, although some information on various reaction cross sections for particular reactions is available.[3] All of the calculated values of the total reaction cross section exceed the lower bound imposed by summing the known partial cross sections.

The role of experimental values of the reaction cross section in determining the optical-model parameters has recently been discussed.[4,29] The dashed contours of constant reaction cross section in Figs. 4–9 represent a quantitative indication of the extent to which a value of σ_r, measured to within a given accuracy, is able to distinguish between volume and surface absorption in terms of b and W.[30] The reaction cross section is related to the optical potential by the relation[31]

$$\sigma_r=-\frac{2}{\hbar v}\int \mathrm{Im}(V_{\mathrm{CN}})|\psi|^2 d^3r, \tag{9}$$

where v is the relative velocity of the incident protons and ψ is the optical-model wave function. It can be shown from (9) that if the optical-model wave function is approximately constant over the nuclear surface, then for a narrow Gaussian surface absorption, the reaction cross section is proportional to the product bW_1.[32] However, Tables II and III reveal that the correlation between bW_1 and σ_r at various energies is only qualitative. Therefore, alterations in the optical-model wave function near the nuclear surface from one energy to the next significantly influence the reaction cross sections, and the (asymptotic) total reaction cross section is not a sensitive index of the nature of the imaginary part of the optical potential. This conclusion is substantiated by observing in Figs. 6 and 8 that the reaction cross section must be known quite accurately in order to remove the surface-volume ambiguity at 14.5 and 15.2 MeV.

D. Polarizations

Published polarization data were available at only one energy, 10 MeV, within the energy range encompassed by the analysis.[12] The optimum fits to this data, analyzed together with the 10.2-MeV differential cross sections, are presented in Fig. 3. The fits to the polarization data, both with and without W_S, are obviously poor. As discussed in NDM, the χ^2 search procedure is less sensitive to the polarizations than to the differential cross sections because of the larger errors in the polarizations. Furthermore, the polarizations are obtained by using much thicker targets than used to measure the cross sections. However, difficulties in obtaining good fits to the polarizations have been experienced previously,[1,23] and their occurrence here was not surprising.

The major discrepancies between the theoretical and experimental polarizations in Fig. 3 are that the theoretical polarizations are too small for $\theta<60°$ and that they lag the experimental values by $\sim 20°$ in the 80°–120° region. These discrepancies are almost identical to those found at 17.8 MeV in the carbon analysis.[1] The

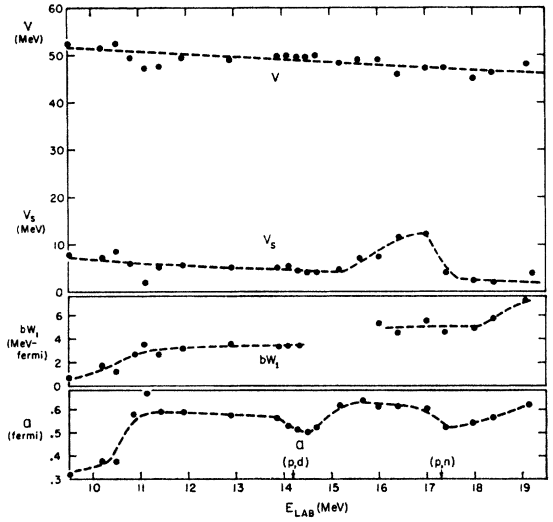

FIG. 11. Energy dependence of the compromise parameters V, V_S, bW_1, and a. The values plotted are obtained from Table III. The threshold energies for the (p,d) and (p,n) reactions are shown by arrows. The values of bW_1 at $E_{lab}=14.5$, 14.7, 15.2, and 15.6 MeV have been omitted as the parameter W is nonzero at these energies.

[29] A. R. Bodner and J. R. Rook, in *Proceedings of the Rutherford Jubilee International Conference, Manchester, 1961*, edited by J. B. Berks (Academic Press Inc., New York, 1961), p. 395. See also, A. R. Bodner and J. R. Rook, Nuclear Phys. 31, 240 (1962).

[30] At all times during the analysis the radii of the real and imaginary potentials were set equal to each other. Contrast the above results to those of Hodgson (reference 4) who introduces an additional parameter by allowing these radii to differ.

[31] See, i.e., R. J. Glauber, *Lectures in Theoretical Physics* (Interscience Publishers, Inc., New York, 1959), Vol. I. p. 324.

[32] J. Olkowsky and J. Raynal, Nucl. Phys. 24, 269 (1961).

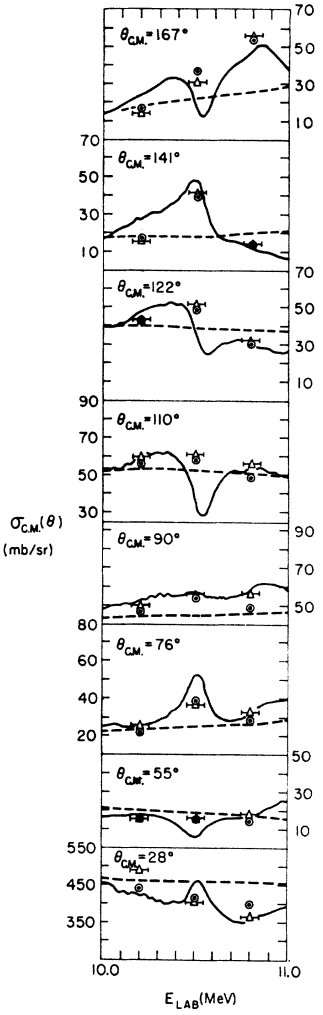

FIG. 12. Comparison of the theoretical and experimental differential cross sections in the 10–11 MeV region. The solid lines are the Wisconsin excitation functions. The triangles are interpolated values from reference 3 with the horizontal bar indicating the quoted energy resolution. The circles are the differential cross sections calculated from the optimum fit parameters. The dashed line results from an optical-model calculation with the compromise parameters: $R_0=1.25$ F, $b=0.6$ F, $a=0.38$ F, $V=51.4$ MeV, $W_1=3.0$ MeV, and $V_S=7.0$ MeV.

tendency of the theoretical polarizations to fall below the experimental values at forward angles was observed also in carbon at 16.2 and 14.0 MeV. In all cases, both in the oxygen and the carbon analyses, the fits to the polarization data could be improved by using smaller values of R_0 than those which yielded the optimum fit to all the data. However, this improvement is achieved only by substantial sacrifice of the quality of the fits to the differential cross sections.[1,33] This difficulty, together with the relative insensitivity of the computed differential cross sections to the value of V_S, indicates that the theoretical polarizations associated with the parameters in Tables II and III (and available upon request) might differ considerably from the experimentally measured quantities. However, the oxygen and carbon analyses demonstrate that improved results would likely be obtained by using as a spin-orbit form factor one which attains the maximum value at smaller radial distances than the Thomas form factor but which maintains sufficiently large values at increasing radial distances to influence the forward-angle scattering. An expanded body of experimental polarizations of protons scattered by oxygen and carbon at energies between 10 and 20 MeV would permit a quantitative test of the above hypothesis within the framework of a systematic analysis of the spin-orbit form factor.

ACKNOWLEDGMENTS

I would like to thank Professor D. S. Saxon, Professor M. A. Melkanoff, and Professor J. S. Nodvik for their hospitality and assistance extended to me on two trips to Los Angeles, and for the subsequent use of their computer program in the present analysis. I am especially grateful to Professor Melkanoff for his assistance in setting up the program in New York and to the staff of the New York University Computing Center for their cooperation during the running of the program. I would also like to thank J. Christenson, W. Daehnick, G. Hardie, and R. Sherr for providing the results of their experiments prior to publication. Finally, it is great pleasure to acknowledge valuable discussions with Professor E. P. Wigner, Professor R. Sherr, Dr. E. Rost, and Dr. W. Daehnick.

[33] G. Hardie (private communication). Reasonable fits to the forward angle p-O polarizations are obtained at 10.2 MeV but at the expense of very poor fits to the differential cross sections.